Differential Shack–Hartmann curvature sensor: local principal curvature measurements

Weiyao Zou,[1,*] Kevin P. Thompson,[2] and Jannick P. Rolland[1]

[1]*CREOL, The College of Optics and Photonics, University of Central Florida, Orlando, Florida 32816, USA*
zouweiyao@gmail.com
[2]*Optical Research Associates, 3280 E. Foothill Blvd., Suite 300, Pasadena, California 91107, USA*
**Corresponding author: zouw@indiana.edu*

Received January 14, 2008; revised June 20, 2008; accepted July 15, 2008;
posted July 22, 2008 (Doc. ID 91598); published August 21, 2008

The concept of a differential Shack–Hartmann (DSH) curvature sensor was recently proposed, which yields wavefront curvatures by measuring wavefront slope differentials. As an important feature of the DSH curvature sensor, the wavefront twist curvature terms can be efficiently obtained from slope differential measurements, thus providing a means to measure the Monge-equivalent patch. Specifically, the principal curvatures and principal directions, four key parameters in differential geometry, can be computed from the wavefront Laplacian and twist curvature terms. The principal curvatures and directions provide a "complete" definition of wavefront local shape. Given adequate sampling, these measurements can be useful in quantifying the mid-spatial-frequency wavefront errors, yielding a complete characterization of the surface being measured.

OCIS codes: 220.4840, 080.0080, 120.6650.

1. MID-SPATIAL-FREQUENCY ERROR MEASUREMENT AND CURVATURE SENSING

Recently, high-accuracy wavefront sensing has been in demand in applications such as high-resolution adaptive optics, or ExAO, and high-accuracy mirror figuring. As the number of elements in an adaptive optic increases, it becomes imperative to sense and recover higher-spatial-frequency errors in the wavefront in addition to the low-spatial-frequency errors. In general, wavefront errors can be categorized into three groups: the low-spatial-frequency errors that contribute to the core of the point-spread function, the mid-spatial-frequency errors that contribute as noise to closely adjacent point-spread functions, and the high-spatial-frequency errors that create a nearly constant background across the sensor. If we define the wavefront errors below 6 cycles per aperture as the low-spatial-frequency errors and those above 20 cycles per aperture as the high-spatial-frequency errors, then the mid-spatial-frequency errors are defined to lie between these two values. Most of the existing wavefront sensing techniques focus on the recovery of the low-spatial-frequency errors. In order to achieve the next level of functionality in wavefront sensing, we need to recover the mid-spatial-frequency errors.

The measurement of the mid-spatial-frequency errors of a mirror surface can be achieved with profilometry. A technique that measures the test surface curvature on a point-by-point basis was first proposed and implemented by Glenn [1]. His method simultaneously measures the local slope at two slightly displaced surface locations with optical probes to obtain the surface slope differentials. This technique was further developed by Weingaertner *et al.* as the large area curvature scanning (LACS) method that used an extended-area optical probe to replace the point-sized optical probe [2–4]. By scanning the test surface, a profile of curvature was built, and the height profile could be deduced. This technique demonstrates subangstrom accuracy and $\lambda/1000$ sensitivity with the differential distance of 0.3 mm and a sample spacing of 10 μm on a 10 mm test piece [5].

For a discrete wavefront-based test, assuming adequate spatial sampling, the accuracy of wavefront estimation depends on how much information is known about the wavefront local shape. For the second-order approximation, the shape parameters most commonly measured for a wavefront local patch include the Laplacian curvatures (c_{xx} and c_{yy}), the average slopes (s_x and s_y), and an average piston value d [6–8]. Given that curvature sensing is a means to achieve vibration-insensitive measurements, curvature sensing is highly desirable when seeking to reach a higher accuracy. In this paper, we focus on intrinsic shape–parameter measurements in characterizing the wavefront local shape, which are the principal curvatures (κ_1 and κ_2) and the principal directions (θ_1 and θ_2).

Curvature, the rate of the surface normal change, is an intrinsic parameter of surface shape. Unlike the slopes (gradients or the first-order derivatives of shape) that vary with changes in surface orientation, the curvature is insensitive to tip/tilt and whole body movement of a surface. The slope measurement at a local patch is a linear approximation of a surface with a tangential plane, while the curvature (the second derivative of shape) is a quadratic approximation of a surface with an osculating quadric spherical surface patch [9]. Thus, in terms of

wavefront local shape estimation, curvature measures provide higher-frequency information about wavefront local shape.

While the Laplacian curvature (in the x or y direction) is defined as the derivative of the wavefront slope along the same direction of slope, a twist curvature term is defined as the derivative of the wavefront slope (e.g., the x slope) that is perpendicular to the slope direction (i.e., the y direction). If we rotate the normal plane at a surface local patch about its normal line, the normal curvature will change and reach its two extreme values: a maximum and a minimum. The wavefront principal curvatures are defined as the maximum and the minimum normal curvatures at a given wavefront patch. The directions of the maximum and the minimum curvatures are orthogonal in space, which are called the principal directions. The wavefront curvatures along the principal directions are simply the principal curvatures, and along the local coordinate frame aligned with the principal directions, the twist curvature terms reduce to zero. Principal curvatures and principal directions are two pairs of important parameters for characterizing the surface local shape in differential geometry and have many applications in computer vision and computer graphics.

While the Laplacian measurements at a local patch approximate the surface with an osculating spherical surface, the principal curvature measurements approximate the surface with an osculating paraboloidal patch, which provides a better estimation of wavefront local shape. The local principal directions do not generally fall along the x and y directions. The knowledge of the principal curvatures and directions allows us to compute the Laplacian curvatures along an arbitrary direction, but the reverse is not true. The principal curvatures and directions provide more freedom in characterizing wavefront local shape. That is an essential merit of principal curvature measurements toward wavefront mid-spatial-frequency error recovery.

There are sensors available for measuring wavefront local slopes and Laplacian curvatures, such as the Shack–Hartmann slope sensor [10], the pyramid wavefront slope sensor [11], and Roddier's Laplacian curvature sensor [6]. The methodologies for wavefront estimation from slopes or Laplacian curvatures or both have been established. However, none of them could provide real-time measurements of wavefront local twist curvature terms, and the definition of the wavefront local shape is incomplete without them. In this paper, we will show how to perform wavefront slope differential measurements in the x and y directions to simultaneously obtain the wavefront twist curvature and Laplacian curvature terms, from which the wavefront local principal curvatures and principal directions may be computed.

2. REVIEW OF PREVIOUS WORK

Several techniques have been developed for curvature-based wavefront sensing [6–8]. Among them, the curvature sensor proposed by Roddier [6] and the hybrid curvature sensor proposed by Paterson and Dainty [7] can provide Laplacian curvatures plus the slope boundary conditions, which are required for solving a Neumann's boundary problem. The coherent gradient sensing technique proposed by Tippur extracts the wavefront curvature information from the gradient field by the finite-difference method [8]. However, none of the previous techniques can provide simultaneously two-dimensional (2-D) measurements of the wavefront Laplacian curvature and twist curvature terms from which the principal curvatures and directions can be extracted. The differential Shack–Hartmann (DSH) curvature sensor was proposed and is being developed to enable such measurements [12,13].

The idea of a differential measurement has been exemplified by the technique called differential image motion monitor (DIMM), a well-known method for measuring atmospheric seeing in astronomy [14,15]. Because DIMM measures the difference in the wavefront tilts over two subapertures some distance apart, it has the advantage of being insensitive to vibration and tracking errors. In this paper we shall show how the DSH simultaneously measures the wavefront Laplacian and twist curvature terms in a 2-D manner. Such a technique, because it is curvature based, is proved to be vibration insensitive.

3. DIFFERENTIAL SHACK–HARTMANN CURVATURE SENSOR

Given a wavefront $W(x,y)$ in a coordinate system with two arbitrary but orthogonal directions as the x and y axes, the Shack–Hartmann sensor provides wavefront slope information by comparing the Hartmann grid coordinates of the measurement beam and the reference beam [10], as shown in Fig. 1. The wavefront slopes in the x and y directions at each Hartmann grid point can be obtained by

$$\left.\frac{\partial W}{\partial x}\right|_i = \frac{x_i^{mea} - x_i^{ref}}{f},$$

$$\left.\frac{\partial W}{\partial y}\right|_i = \frac{y_i^{mea} - y_i^{ref}}{f}, \tag{1}$$

where (x_i^{ref}, y_i^{ref}) and (x_i^{mea}, y_i^{mea}) $(i=1,2,\ldots,m$, and $m=t \times t$ is the total number of grid points) are the Hartmann grid coordinates of the reference beam and the measurement beam, respectively, and f is the focal length of the lenslet array. As a slope sensor, it is sensitive to rigid body rotations and displacements of the surface under test, and thus such a technique is well known to be vibration sensitive

The DSH curvature sensor builds on the conventional Shack–Hartmann sensor with the collimated beam split

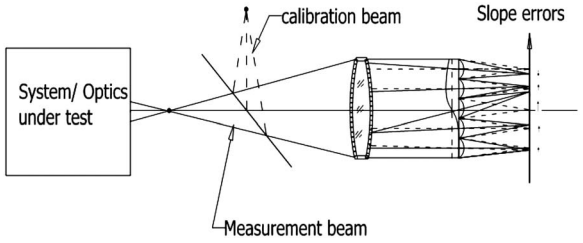

Fig. 1. Concept of the Shack–Hartmann wavefront sensor.

into three channels to yield three wavefronts exactly the same as one another. As shown in Fig. 2, measuring the differentials of the wavefront slopes along the x or y direction will yield the wavefront curvature along that direction, which can be implemented by measuring two slopes simultaneously over a given lateral differential distance on the wavefront grid. A lenslet array is mounted in each channel at the image position of the optical system entrance pupil generated by a pupil relay lens. As shown in Fig. 3, the lenslet array in the z direction is conjugated to each of the other two by beam splitters. Shearing devices make two of the three Hartmann grids displaced two differential distances in the x and y directions independently with respect to the third one. Irradiance detection devices, such as CCD cameras, may be used to record the beamlet centroidal positions relative to the Hartmann grid coordinates defined by the CCD pixel positions. As a most important feature of the DSH curvature sensor, it can measure both the twist curvature terms and the Laplacian curvature terms required for computing the principal curvatures and principal directions.

As illustrated in Fig. 2, the slope differentials in the x and y directions can be computed as

$$c_{xx}(i) = \left.\frac{\partial^2 W}{\partial x^2}\right|_i = \frac{1}{s_x}\left(\left.\frac{\partial W}{\partial x}\right|_{i'} - \left.\frac{\partial W}{\partial x}\right|_i\right) = \frac{1}{f}\left(\frac{x_i'^{mea} - x_i^{mea}}{s_x}\right) - c_{0,xx}(i),$$

$$c_{yy}(i) = \left.\frac{\partial^2 W}{\partial y^2}\right|_i = \frac{1}{s_y}\left(\left.\frac{\partial W}{\partial y}\right|_{i''} - \left.\frac{\partial W}{\partial y}\right|_i\right) = \frac{1}{f}\left(\frac{y_i''^{mea} - y_i^{mea}}{s_y}\right) - c_{0,yy}(i), \quad (2)$$

where s_x and s_y are the differential grid shears in the x and y directions, respectively, and the constants $c_{0,xx}(i)$ and $c_{0,yy}(i)$ are given by

$$c_{0,xx}(i) = \frac{1}{f}\left(\frac{x_i'^{Ref} - x_i^{Ref}}{s_x}\right),$$

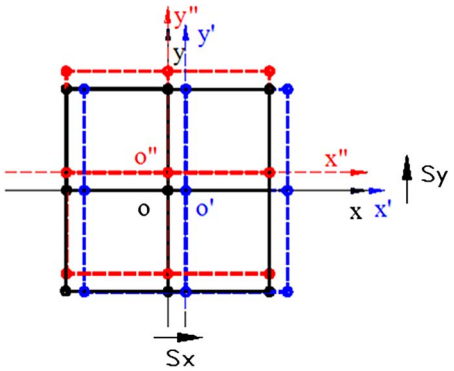

Fig. 2. (Color online) The x- and y-differential shears of the Hartmann grid.

$$c_{0,yy}(i) = \frac{1}{f}\left(\frac{y_i''^{Ref} - y_i^{Ref}}{s_y}\right). \quad (3)$$

The twist curvature terms are the slope differentials in the cross directions, which can be obtained by

$$c_{xy}(i) = \left.\frac{\partial^2 W}{\partial x \partial y}\right|_i = \frac{1}{s_x}\left(\left.\frac{\partial W}{\partial y}\right|_{i'} - \left.\frac{\partial W}{\partial y}\right|_i\right) = \frac{1}{f}\left(\frac{y_i'^{mea} - y_i^{mea}}{s_x}\right) - c_{0,xy}(i),$$

$$c_{yx}(i) = \left.\frac{\partial^2 W}{\partial y \partial x}\right|_i = \frac{1}{s_y}\left(\left.\frac{\partial W}{\partial x}\right|_{i''} - \left.\frac{\partial W}{\partial x}\right|_i\right) = \frac{1}{f}\left(\frac{x_i''^{mea} - x_i^{mea}}{s_y}\right) - c_{0,yx}(i), \quad (4)$$

where $c_{0,yx}(i)$ and $c_{0,xy}(i)$ are constants given by

$$c_{0,xy}(i) = \frac{1}{f}\left(\frac{y_i'^{Ref} - y_i^{Ref}}{s_x}\right),$$

$$c_{0,yx}(i) = \frac{1}{f}\left(\frac{x_i''^{Ref} - x_i^{Ref}}{s_y}\right). \quad (5)$$

In Eqs. (2)–(5), (x_i^{mea}, y_i^{mea}), $(x_i'^{mea}, y_i'^{mea})$, and $(x_i''^{mea}, y_i''^{mea})$ $(i=1,2,\ldots,m)$ are the coordinates of the measurement beam at the original Hartmann grid, the x-sheared, and the y-sheared Hartmann grids, respectively; (x_i^{Ref}, y_i^{Ref}), $(x_i'^{Ref}, y_i'^{Ref})$, and $(x_i''^{Ref}, y_i''^{Ref})$ $(i=1,2,\ldots,m)$ are the corresponding coordinates of the reference beam.

Theoretically, $c_{0,xx}$ and $c_{0,yy}$ should both be "$1/f$," and $c_{0,xy}$ and $c_{0,yx}$ should both be zero for the second-order approximation. However, they all need to be calibrated in practice, as the three CCD cameras used in the three measurement channels are different from one to another. In the experimental setup shown in Fig. 3, a reference light beam is introduced to generate the reference Hartmann grid arrays for the three channels, and the constants $c_{0,xx}$, $c_{0,yy}$, $c_{0,xy}$, and $c_{0,yx}$ can be computed with Eqs. (3) and (5). To make the principal curvature measurements unique, it is assumed that the twist curvature terms are equal, i.e., $c_{xy}=c_{yx}$.

4. COMPUTATION OF PRINCIPAL CURVATURES AND DIRECTIONS

Given the measurements of the Laplacian curvatures and twist curvature terms, we will show how to compute the principal curvatures (say, κ_1 and κ_2) and directions. Considering a local surface patch, the principal curvatures are invariants that are insensitive to the surface orientation change. In order to evaluate the principal curvatures, we assume that the local wavefront patch is represented by a "Monge patch" of the form

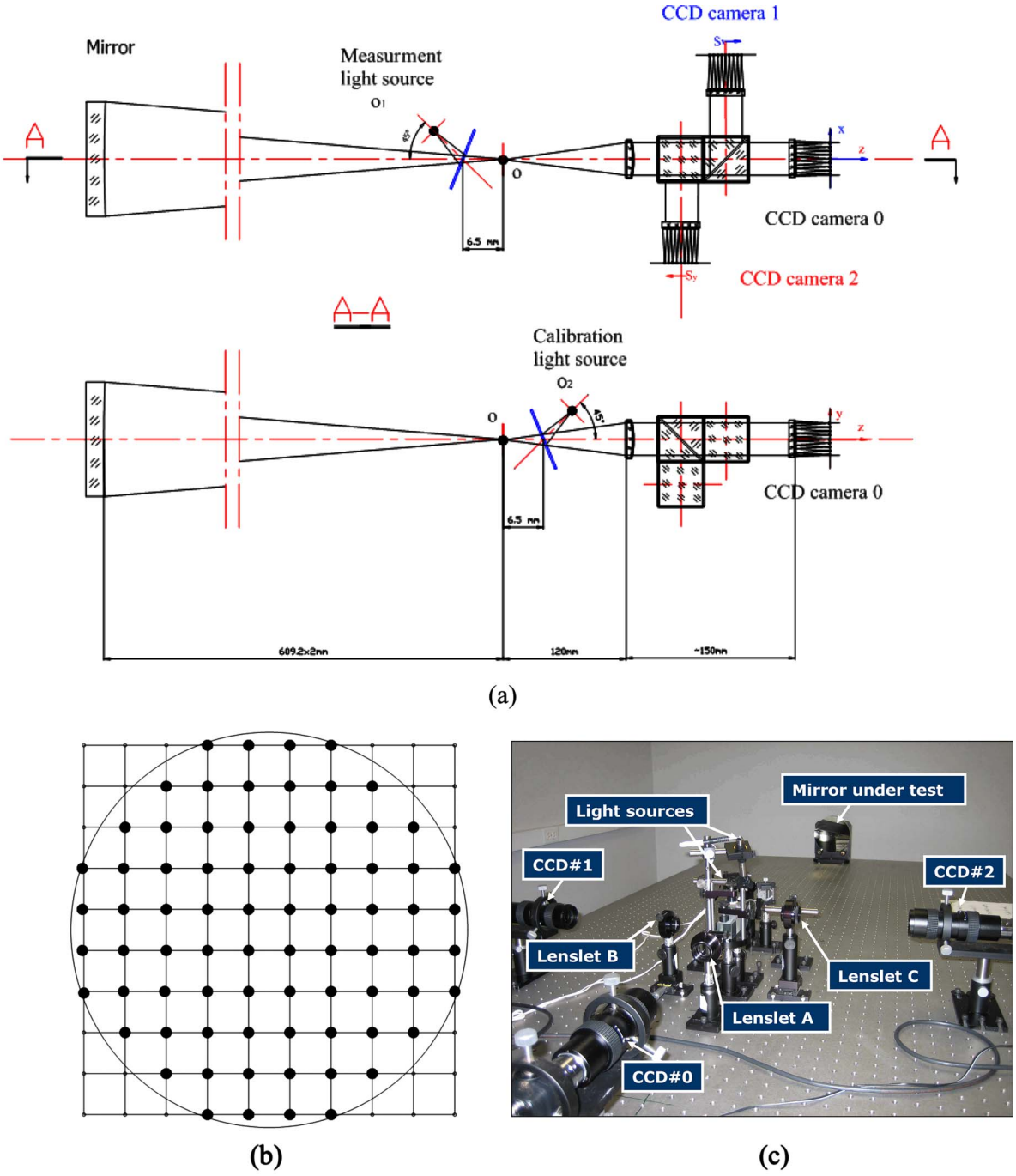

Fig. 3. (Color online) Experimental system of a possible implementation for the differential Shack–Hartmann curvature sensor: (a) (color online) optical layout, (b) Hartmann sampling grid, (c) (color online) picture of the experimental system.

$$\mathbf{X} = x\vec{e}_1 + y\vec{e}_2 + W(x,y)\vec{e}_3, \tag{6}$$

where $(\vec{e}_1, \vec{e}_2, \vec{e}_3)$ is an orthogonal frame in 3-D Euclidean space. To describe the local surface shape, the Second Fundamental Form has a matrix form as [16]

$$\mathbf{II} = \begin{pmatrix} \hat{\omega}_1^{13} & \hat{\omega}_1^{23} \\ \hat{\omega}_2^{13} & \hat{\omega}_2^{23} \end{pmatrix}, \tag{7}$$

where $\hat{\omega}_j^{i3}(i=1,2;j=1,2)$ defines the component in $\vec{e}_i$ of the turning rate of the normal as the frame is moved across the given point along $\vec{e}_j$. For a wavefront traveling in the z direction $(\vec{e}_3)$, $W(x,y)$ is the "height" as a function of x and y in the pupil plane. Then, at each "Monge patch," the matrix **II** becomes

$$\mathbf{II} = \begin{pmatrix} c_{xx}(i) & c_{yx}(i) \\ c_{xy}(i) & c_{yy}(i) \end{pmatrix}, \qquad i = 1,2,\ldots,m. \tag{8}$$

The determinant of matrix **II**, denoted as $K=c_{xx}c_{yy}-c_{xy}c_{yx}$, is known as the local wavefront Gaussian curvature. The trace of the matrix **II**, denoted as $2H$, is the local wavefront Laplacian, where $H=(c_{xx}+c_{yy})/2$ is known as the local wavefront mean curvature. Both Gaussian curvature and mean curvature (or Laplacian curvature)

are algebraic invariants, which do not change with rotation of the orthogonal frame $(\vec{e}_1, \vec{e}_2, \vec{e}_3)$ about the normal [9].

Within this mathematical framework, the principal curvatures are the eigenvalues of the matrix of the Second Fundamental Form, and the principal directions are their corresponding eigenvectors [9,16]. By diagonalizing the matrix of the Second Fundamental Form, the principal curvatures can be computed from the twist curvature and the Laplacian curvatures terms [16].

To diagonalize the matrix $\mathbf{II}$ is to rotate the orthogonal frame about axis $\vec{e}_3$ to make the off-diagonal terms disappear. Then we obtain a new matrix $\mathbf{II}'$ by

$$\mathbf{II}' = \mathbf{P}^{\mathbf{T}}\mathbf{II}\mathbf{P}, \tag{9}$$

where $\mathbf{P}$ is an orthogonal matrix defined by

$$\mathbf{P} = \begin{bmatrix} \cos\theta & -\sin\theta \\ \sin\theta & \cos\theta \end{bmatrix}, \tag{10}$$

where the angle θ is defined as the frame rotation angle. The new matrix $\mathbf{II}'$ is a diagonal matrix, which is

$$\mathbf{II}' = \begin{pmatrix} \kappa_1(i) & 0 \\ 0 & \kappa_2(i) \end{pmatrix}, \tag{11}$$

where $\kappa_1(i)$ and $\kappa_2(i)(\kappa_1(i) \geqslant \kappa_2(i))$ are the eigenvalues of the matrix $\mathbf{II}$, also known as the first and second principal curvatures, and $i = 1, 2, \ldots, m$, where m is the total number of Shack–Hartmann grid points. Combining the results of Eqs. (8)–(11), the principal curvatures κ_1 and κ_2 may be obtained at each grid point by

$$\kappa_{1,2}(i) = \frac{c_x(i) + c_y(i) \pm \sqrt{(c_x(i) - c_y(i))^2 + 4c_{xy}(i)^2}}{2}, \tag{12}$$

with the rotation angle θ between the first principal curvature and the x direction is given by

$$\theta(i) = \frac{1}{2}\tan^{-1}\left(\frac{2c_{xy}(i)}{c_x(i) - c_y(i)}\right). \tag{13}$$

The principal curvatures can also be computed by evaluating the eigenvalues of the matrix $\mathbf{II}$ with its characteristic equation given by

$$\det(\kappa\mathbf{I} - \mathbf{II}) = 0. \tag{14}$$

The result is the same as Eq. (12).

According to the Euler curvature formula (1760) [9], the Laplacian curvature in the x direction can be expressed as

$$c_x(i) = \kappa_1(i)\cos^2[\theta(i)] + \kappa_2(i)\sin^2[\theta(i)]. \tag{15}$$

Then the rotation angle θ can also be computed by

$$\cos 2[\theta(i)] = \frac{2c_x(i) - 2H(i)}{\kappa_1(i) - \kappa_2(i)}, \tag{16}$$

where H is the mean curvature. Then the angle θ is given by

$$\theta(i) = \frac{1}{2}\cos^{-1}\left(\frac{c_x(i) - c_y(i)}{\kappa_1(i) - \kappa_2(i)}\right). \tag{17}$$

Substituting Eq. (12) into Eq. (17), we obtain

$$\theta(i) = \frac{1}{2}\cos^{-1}\left(\frac{|c_x(i) - c_y(i)|}{\sqrt{(c_x(i) - c_y(i))^2 + 4c_{xy}(i)^2}}\right), \tag{18}$$

which is equivalent to Eq. (13).

5. SYSTEM IMPLEMENTATION AND EXPERIMENTAL RESULTS

An experimental system for an implementation of the DSH curvature sensor is shown in Fig. 3 [12,17], where two micrometer-level displacement mechanisms are used to make the lateral differential shears of the Hartmann grid in the x and y directions. The shearing distance is about 1/6–1/8 of the pitch size of the Shack–Hartmann grid. The optical layout of the sensor combined with a commercial quality mirror with a working f-ratio of $f/6$ is illustrated in Fig. 3, which is used to generate a sample wavefront for principal curvature measurements. Following the output beam, which is collimated by an achromatic lens, two cube beam splitters are used to split the output beam into three channels. As a proof-of-concept system, a 10×10 lenslet array with the pitch size of 1.79×1.79 mm^2 and focal lengths of 90 mm were used to generate a Hartmann grid in each channel [18]. The point light source O_1 is the measurement light source, and O_2 is the reference light source. After calibration, no reference light beam is needed in this system, and all the systematic errors cancel out except for the discrepancy errors among the lenslet arrays (usually negligible), the errors from the first surface mirror that introduces the reference light, and the error from the beam splitter that introduces the measurement light, which need to be considered in practice.

Figure 4 shows a result for wavefront principal curvatures and principal directions estimated from curvature (i.e., Laplacian and twist) measurements. The solid lines with an arrow on each end represent the first principal curvatures and directions, while the dotted lines with an arrow on each end represent the second principal curvatures and directions. The lengths of these lines represent the values of the principal curvatures. The principal curvature map in Fig. 4 is shown to agree with the wavefront shape estimated from slope data.

6. DISCUSSION AND CONCLUSION

Since the DSH curvature sensor is derived from the Shack–Hartmann slope sensor, it shares the important features of the Shack–Hartmann slope sensor, while it adds the important features of a curvature sensor. Compared with previous techniques, the DSH curvature sensor provides an efficient and convenient way to measure wavefront local twist curvature terms in addition to the Laplacian curvature terms from which the local principal curvatures and directions can be estimated. To our knowledge, the DSH curvature sensor is the first instrument to provide real-time measurements of wavefront twist cur-

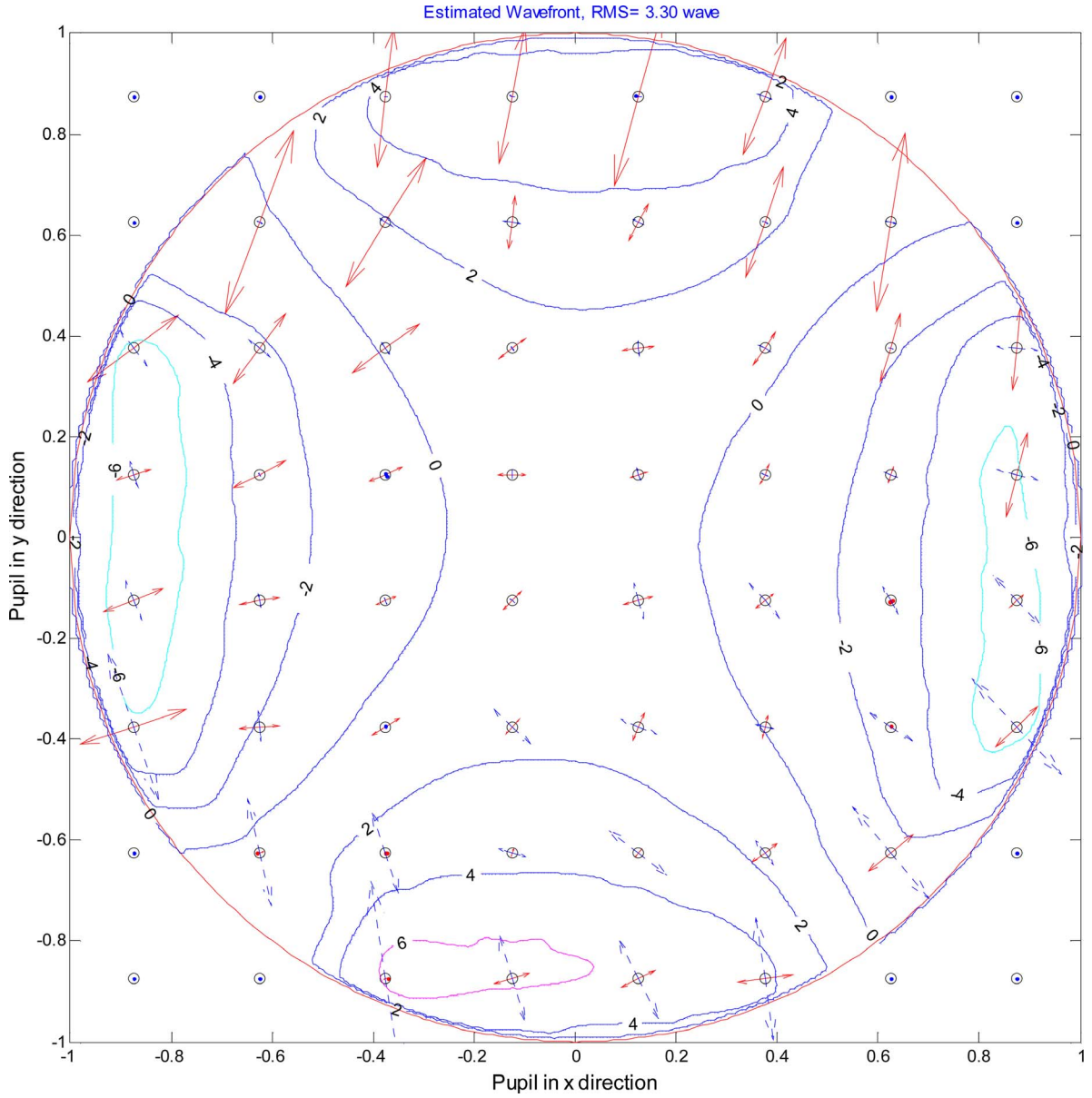

Fig. 4. (Color online) Map of the principal curvatures and principal directions on a wavefront estimated from the measured slope data (arrow length scale=0.6). Solid arrow lines, first principal curvatures and directions; dotted arrow lines, second principal curvatures and directions.

vatures, wavefront principal curvatures, and wavefront principal directions beyond the Laplacian curvatures.

The DSH curvature sensor employs a Shack–Hartmann with three channels and loses 75% of light irradiance on the CCD camera, but it yields ten parameters about wavefront local shape: the wavefront slopes in the x and y directions (s_x and s_y), the Laplacian curvatures in the x and y directions (c_{xx} and c_{yy}), the twist curvature terms (c_{xy} and c_{yx}), the principal curvatures (κ_1 and κ_2), and the principal directions (θ_1 and θ_2). According to the analysis provided by Hardy and Guyon [19,20], the root-mean-square (RMS) value of the CCD centroiding noise is in inverse proportion to the square root of the number of photons collected per subaperture. The DSH curvature sensor collects only 25% of the photons per subaperture as compared with a regular Shack–Hartmann sensor; therefore the RMS value of the CCD centroiding error doubles. However, in some metrology applications, the beam intensity of the wavefront under test can be increased to be adequately high, and the irradiance reduction in the DSH sensor is no longer a limit for the CCD centroiding accuracy.

In Roddier's curvature sensor, the determination of the defocus distance and focal plane is affected by the seeing blur and the caustic zone, especially for the slow f-ratios [21], which makes the Laplacian measurements less accurate and less convenient. In the DSH curvature sensor, the slope differential measurements are performed at the pupil plane of the optical system under test, so the difficulties associated with operations close to the caustic zone as in Roddier's curvature sensor are avoided.

The DSH curvature sensor is derived from the Shack–Hartmann slope sensor, and its wavefront phase estimation does not depend on the wavelength of the testing

light. Therefore it does not have a "2π-ambiguity" problem in wavefront estimation, while most of the irradiance-based phase retrieval methods do. This feature allows the DSH curvature sensor to work well with large aberrations.

Usually, vibration noise is the limiting factor for high-accuracy wavefront estimation, especially for the mid-spatial-frequency recovery. Compared with a slope sensor, the DSH sensor measures Laplacian curvatures and twist curvatures terms that are insensitive to all types of vibrations and drifts, both in surface height and in surface slope. Moreover, the slope differential measurements in the DSH curvature sensor are performed simultaneously in 2D, so the scanning errors as in profilometry are avoided.

In summary, a "complete" measurement of wavefront local shape, which extends the surface characterization obtained in a single measurement to include both low- and mid-spatial-frequency errors, is needed to support the advancing density of actuators in adaptive component optical systems. The DSH curvature sensor presented here for the first time provides this capability. The essential merit of the DSH curvature sensor over a common Laplacian curvature sensor is its superior estimation of wavefront local shape. The principal curvatures and directions construct an osculating paraboloidal surface patch that provides a more accurate description of local wavefront shape when compared with the two osculating spherical surfaces that are derived from the Laplacian curvatures. Based on the above discussion and given that the slope and Laplacian-based wavefront sensing techniques are popular today, we can expect that principal-curvature-based wavefront sensing will in the future contribute much across many applications.

ACKNOWLEDGMENTS

This work was funded in part by the National Science Foundation grant IIS/HCI-0307189. We thank Paul Glenn for sharing his experience on his 1-D curvature sensor development. The authors thank Stephen A. Burns for his stimulating comments about the manuscript, and we are thankful to the reviewers of JOSA A for their constructive comments.

REFERENCES

1. P. E. Glenn, "Robust, sub-angstrom level mid-spatial frequency profilometry," Proc. SPIE **1333**, 230–238 (1990).
2. I. Weingaertner, M. Schulz, and C. Elster, "Novel scanning technique for ultra-precise measurement of topography," Proc. SPIE **3782**, 306–317 (1999).
3. M. Schulz, "Topography measurement by a reliable large-area curvature sensor," Optik (Stuttgart) **112**, 86–90 (2001).
4. I. Weingaertner, M. Schulz, P. Thomsen-Schmidt, and C. Elster, "Measurement of steep aspheres: a step toward nanometer accuracy," Proc. SPIE **4449**, 195–204 (2001).
5. P. Glenn, "Angstrom level profilometry for sub-millimeter to meter scale surface errors," Proc. SPIE **1333**, 326–336 (1990).
6. F. Roddier, "Curvature sensing and compensation: a new concept in adaptive optics," Appl. Opt. **27**, 1223–1225 (1988).
7. C. Paterson and J. C. Dainty, "Hybrid curvature and gradient wave-front sensor," Opt. Lett. **25**, 1687–1689 (2000).
8. H. V. Tippur, "Coherent gradient sensing: a Fourier optics analysis and applications to fracture," Appl. Opt. **31**, 4428–4439 (1992).
9. J. J. Koenderink, *Solid Shape* (MIT, 1990), pp. 210, 214, 212, 228, 232.
10. R. V. Shack and B. C. Platt, "Production and use of a lenticular Hartmann screen," J. Opt. Soc. Am. **61**, 656 (1971).
11. R. Ragazzoni, "Pupil plane wavefront sensing with an oscillating prism," J. Mod. Opt. **43**, 289–293 (1996).
12. W. Zou and J. Rolland, "Differential wavefront curvature sensor," Proc. SPIE **5869**, 5869171 (2005).
13. W. Zou and J. Rolland, "Differential Shack–Hartmann curvature sensor," U.S. patent 7,390,999 (24 June 2008).
14. M. Sarazin and F. Roddier, "The ESO differential image motion monitor," Astron. Astrophys. **227**, 294–300 (1990).
15. A. Tokovinin, "From differential image motion to seeing," Publ. Astron. Soc. Pac. **114**, 1156–1166 (2002).
16. V. Interrante, H. Fuchs, and S. M. Pizer, "Conveying the 3D shape of smoothly curving transparent surface via texture," IEEE Trans. Vis. Comput. Graph. **3**, 98–117 (1997).
17. W. Zou, "Optimization of zonal wavefront estimation and curvature measurements," Ph.D. dissertation (University of Central Florida, 2007).
18. Adaptive Optics Associates Inc., part no. 1790–90-s, http://www.aoainc.com/index.html.
19. O. Guyon, "Limits of adaptive optics for high-contrast imaging," Astrophys. J. **629**, 592–614 (2005).
20. J. Hardy, *Adaptive Optics for Astronomical Telescopes* (Oxford U. Press, 1998).
21. C. Roddier and F. Roddier, "Wave-front reconstruction from defocused images and the testing of ground-based optical telescopes," J. Opt. Soc. Am. A **10**, 2277–2287 (1993).